

Universal set of scalable dynamically corrected gates for quantum error correction with always-on qubit couplings

Amrit De and Leonid P. Pryadko

Department of Physics & Astronomy, University of California, Riverside, California 92521

(Dated: November 22, 2021)

We construct a universal set of high fidelity quantum gates to be used on a sparse bipartite lattice with always-on Ising couplings. The gates are based on dynamical decoupling sequences using shaped pulses, they protect against low-frequency phase noise, and can be run in parallel on non-neighboring qubits. This makes them suitable for implementing quantum error correction with low-density parity check codes like the surface codes and their finite-rate generalizations. We illustrate the construction by simulating quantum Zeno effect with the $[[4, 2, 2]]$ toric code on a spin chain.

Quantum error correction (QEC) makes it theoretically possible to perform large quantum computations with a finite per-qubit error rate[1–3]. In practice QEC is extremely difficult since the corresponding *error probability threshold* is small[4–9]. When only local interactions between the qubits are allowed, the estimated threshold value is the highest, around 1%, for toric and related surface codes[5, 9, 10]. However, as to how to implement the operations efficiently and with the required accuracy, is an open question.

Qubits with always-on couplings are a natural model for several potential quantum computer (QC) architectures currently under investigation. On general grounds, compared to their counterparts with tunable couplings, such qubits can be expected to have better parameter stability and longer coherence times. In addition, over sixty years of development in nuclear magnetic resonance (NMR) yielded an amazing degree of control available to such systems[11, 12]. Related techniques based on selective dynamical decoupling(DD) of parts of the system Hamiltonian with carefully designed pulse sequences have been further developed in application to quantum computation[13–19].

While NMR quantum computation is not scalable[20], it still holds several records for a number of coherently controlled qubits[12]. However, some of these have been achieved with the help of the *strongly-modulated* pulses, computer-generated single- and multi-qubit gates tailored for a particular system Hamiltonian[21–24]. While such gates can be used in other QC architectures[25], they may violate the scalability.

On the other hand, NMR-inspired techniques like DD can also be used to control large systems with local interactions, with the scalability achieved by designing pulses and sequences to a given order in the Magnus series[26] on small qubit clusters[27, 28]. DD is also excellent in producing accurate control for systems where not all interactions are known as one can decouple interactions with the given symmetry[29, 30]. Moreover, DD works best against errors coming from low-frequency bath degrees of freedom which tend to dominate the decoherence rates, and it does not require additional qubits. In short,

DD is an excellent choice for the first level of coherence protection; it’s use could greatly reduce the required repetition rate of the QEC cycle.

This is well recognized in the community and applications of DD for QC are actively investigated by a number of groups. However, most publications on the subject illustrate general principles using a single qubit as an example, leaving out the issues of design and simulation of scalable approaches to multi-qubit dynamical decoupling. While the techniques for larger systems exist, they typically yield longer decoupling sequences[17, 29, 31].

THE GOAL OF THIS WORK is to provide a scalable benchmark implementation of a universal set of accurate gates using soft pulses for a system with always-on qubit couplings. Specifically, we construct one- and two-qubit gates with built-in DD-protection against low-frequency phase noise for a sparse bipartite lattice of qubits with the nearest-neighbor (n.n.) Ising couplings. The constructed gates use finite-amplitude *shaped pulses* which can be implemented experimentally. They are *scalable*, in the sense that the same construction works for an arbitrary lattice, and they can also be executed *in parallel* for different qubits and/or qubit pairs. This makes them ideal for implementing QEC with quantum low-density parity check (LDPC) codes[32, 33], in particular, the surface codes and their finite-rate generalizations[5, 34, 35]. In the limit of very slow (classical) bath the gates are accurate to second order in the Magnus expansion, meaning that their infidelity scales as sixth or higher powers of the coupling, in units of inverse pulse duration. We demonstrate the accuracy of the constructed gates by simulating the quantum Zeno effect[36, 37] repeatedly for the $[[4, 2, 2]]$ error-detecting toric code on an Ising chain. The simulations are done with five qubits, using classical correlated noise as a source of dephasing.

Two techniques are essential to our work. First, the use of NMR-style self-refocusing pulses[27, 38–40], which (to a given order) work as drop-in replacement for hard, δ -function-like pulses. In simulations, we use the second-order pulses designed and characterized in Refs. 27, 28, 39, and 41. The second technique is the Eulerian path construction for generating accurate DD sequences[16],

and its extension, the dynamically corrected gates[31, 42, 43] which allow for the construction of composite pulses accurate to a given order of the Magnus expansion.

WE CONSTRUCT OUR GATES for a collection of qubits arranged on an arbitrary sparse bipartite graph \mathcal{G} with edge set \mathcal{E} , with an Ising coupling for every edge,

$$H_S \equiv \frac{1}{2} \sum_{(ij) \in \mathcal{E}} J_{ij} \sigma_i^z \sigma_j^z, \quad (1)$$

arbitrary (within the bandwidth) single-qubit control,

$$H_C \equiv \frac{1}{2} \sum_i \sum_{\mu=x,y,z} \sigma_i^\mu V_{i\mu}(t), \quad (2)$$

in the presence of low-frequency phase noise

$$H_N \equiv \frac{1}{2} \sum_i \sigma_i^z B_i + H_B, \quad (3)$$

where the bath coupling operators B_i can result, e.g., from low-frequency phonons, or nuclear spins, and their dynamics is governed by the bath Hamiltonian H_B independent from σ_i^μ .

Decoherence resulting from higher-frequency bath modes, e.g., described by the Lindblad equation[44], can be also introduced, but at later design stages, since DD is not effective against such decoherence. While we do not consider Markovian decoherence here, we mention in passing that the main effects of DD are the suppression of equilibrium population asymmetries (qubits are constantly flipped), and, with soft-pulse DD, the redistribution of decoherence rates between the channels[41]. For example, even if dephasing is dominant for non-driven qubits, any sequence of finite-width pulses creates some longitudinal relaxation (compensated by a reduction of the dephasing rate).

To construct the CNOT gate, we use the identity [45]

$$\text{CNOT}_{cd} = e^{i\pi/4} Y_c \bar{X}_c \bar{Y}_c X_d \bar{Y}_d e^{-i\pi/4} \sigma_c^z \sigma_d^z Y_d, \quad (4)$$

where $X_i \equiv \exp(-i\frac{\pi}{4}\sigma_i^x)$, $Y_i \equiv \exp(-i\frac{\pi}{4}\sigma_i^y)$, are $\pi/2$ unitaries, and \bar{X}_i , \bar{Y}_i denote the corresponding conjugate gates [in simulations we use the equivalent form with $Y_c \bar{X}_c \bar{Y}_c \equiv Z_c$].

TO IMPLEMENT THE TWO-QUBIT zz -rotation gate, $e^{-i\pi/4\sigma_c^z \sigma_d^z}$, we run two period- $16\tau_p$ decoupling sequences on the sublattices A and B , $V_A(t)$ and $V_B(t)$ in Fig. 1, where each pulse of duration τ_p is a symmetric π pulse applied in the x direction. When the pulses are second-order self-refocusing pulses [e.g., $Q_1(\pi)$ from Refs. 27 and 39 shown], these sequences suppress the effect of the Ising couplings H_S and the noise H_N to second order in the Magnus expansion, meaning that the effective Hamiltonian is just H_B , with the error scaling as $\propto \tau_p^2$. This gives the error in the unitary matrix scaling as $\propto \tau_p^3$, and the corresponding infidelity scaling as $\propto \tau_p^6$.

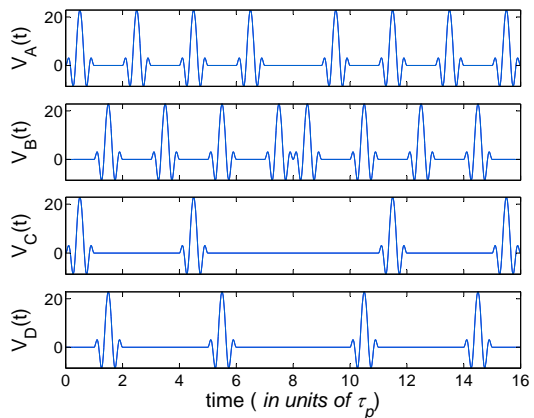


FIG. 1. (color online) Pulse sequences used to implement two-qubit zz -rotations on a bipartite lattice with Ising couplings. Global sequences of π -pulses in x direction $V_A(t)$ and $V_B(t)$ are executed on the idle qubits of the two sublattices. These decouple the inter-qubit Ising couplings and also the single-qubit low-frequency phase noise terms. In order to couple two neighboring qubits, on these qubits the sequences V_A , V_B are replaced by V_C , V_D , respectively. This produces an effective Ising Hamiltonian with half of the original coupling. Shown are $Q_1(\pi)$ second-order self-refocusing pulse shapes[27, 39] used in the simulations.

To turn on the coupling between two neighboring qubits c, d , the two sublattice sequences on these qubits are replaced with $V_C(t)$ and $V_D(t)$, respectively, see Fig. 1. These sequences are chosen so that the Ising coupling between these qubits is only removed half of the time, while the coupling to other qubits continues to be removed. More precisely, with second-order pulses, the effective Hamiltonian is $H_B + (J/4)\sigma_c^z \sigma_d^z + \mathcal{O}(\tau_p^2)$. Repeating this sequence m times gives the system evolution

$$U_{zz} = \exp(-i\alpha\sigma_c^z \sigma_d^z), \quad \alpha = 4mJ\tau_p, \quad (5)$$

with the error scaling as $\propto m\tau_p^3$, where the term associated with the bath evolution is suppressed. Such sequences can be run simultaneously on many pairs of qubits as long as qubits from different pairs are not mutually coupled.

WE IMPLEMENT SINGLE-QUBIT ROTATIONS with the leading-order DCGs[31, 42], using the pulse sequences in Fig. 2. Again, two decoupling sequences, $V_1(t)$ and $V_2(t)$, are run globally on the two sublattices; additional pulses are inserted for the qubits to be rotated [$V_3(t)$ in Fig. 2 shows an implementation of the $\pi/2$ rotation with respect to Y axis on a sublattice-A qubit].

Nominally, DCG guarantees the first-order decoupling with any pulses. However, in our case, the decoupling sequences $V_i(t)$, $i = 1, 2$, do not go over the complete single-qubit groups. Thus, unoptimized (e.g., Gaussian) pulses can produce unitary errors scaling linearly with the pulse duration τ_p ; one needs first-order self-refocusing pulses[27, 38, 39] to get first-order decoupling. In the case of the second-order pulses (e.g., $Q_1(\phi)$ [39]), the remain-

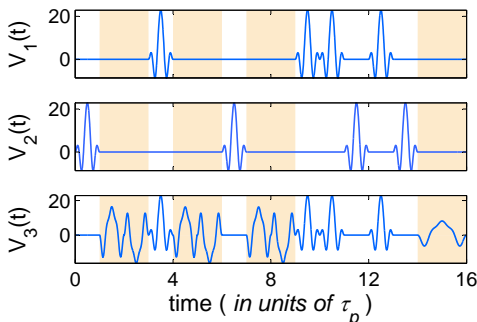


FIG. 2. (color online) Pulse sequence used to implement single-qubit rotations. The sequences of π pulses in x direction, $V_1(t)$ and $V_2(t)$, are executed globally on the idle qubits of the two sublattices. A single-qubit rotation is implemented as a DCG[31, 42] by adding three pulse-antipulse combinations and the stretched pulse in the shaded regions; the sequence $V_3(t)$ where $Q_1(\pi/2)$ pulses in y direction are added corresponds to a $(\pi/2)_Y$ operation on a sublattice-A qubit. Such gates can be executed on any set of non-neighboring qubits.

ing order- τ_p^2 errors are all proportional to different commutators $[B_i, B_j]$ and $[H_B, B_i]$, which gives second-order decoupling (infidelity $\propto \tau_p^6$) when the operators B_i are replaced by c -numbers Δ_i (cf. chemical shifts in NMR).

These accuracy predictions are confirmed in Fig. 3 which shows the average infidelities for a single $(\pi/2)_Y$ rotation of qubit 3 [Fig. 3(a)] and a complete CNOT₂₃ gate [Fig. 3(b)] as a function of the r.m.s. chemical shift Δ (in units of τ_p^{-1}), obtained numerically for a four-qubit Ising chain. The simulations are done with a custom C++ program using fourth-order Runge-Kutta algorithm for integrating the unitary dynamics and the Eigen3 library[46] for matrix arithmetics. We fix the value of $J_{ij} = J = \pi/(16m\tau_p)$ with $m = 5$ repetitions of the basic sequence [see Eqs. (4), (5) and Fig. 1] in the CNOT gate; with the addition of four single-qubit DCGs [see Fig. 2] the CNOT duration is $t_{\text{CNOT}} = 9 \times 16\tau_p = 144\tau_p$. For small Δ , the infidelities are dominated by the decoupling accuracy of the inter-qubit interactions, while they scale as $\propto \Delta^6 \tau_p^6$ for large Δ , see the graphs of the corresponding slopes in the insets.

WE ILLUSTRATE THE PERFORMANCE of the designed gates by simulating the quantum Zeno effect[36, 37] using the four-qubit toric error-detecting code [10, 47]. We used zero-mean classical stationary Gaussian stochastic processes with Gaussian correlations, $\langle B_i(t)B_j(t') \rangle = \sigma^2 \delta_{ij} e^{-(t-t')^2/\tau_c^2}$, as the decoherence source. These are obtained by applying the Gaussian filter to discrete sets of uncorrelated random numbers drawn from the Gaussian distribution, and using the standard cubic spline interpolation with the result.

The $[[4, 2, 2]]$ toric code is a stabilizer code [48, 49] encoding an arbitrary state of $k = 2$ qubits into a 2^2 -dimensional subspace \mathcal{Q} of the 4-qubit Hilbert space. The subspace \mathcal{Q} is the common $+1$ eigenspace of the two *sta-*

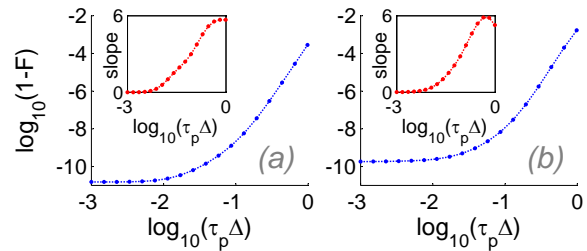


FIG. 3. (color online) (a) The infidelity of the gate in Fig. 2 and (b) the infidelity of the complete C-NOT gate between qubits 2 and 3 of a four-qubit n.n. Ising chain as a function of r.m.s. chemical shift Δ (pulse sequences not shown). For small Δ the errors saturate because of the fixed interqubit coupling J ; for large Δ the errors are dominated by the chemical shifts. The insets show the corresponding slopes; the slope of approximately 6 [infidelity $\propto (\tau_p \Delta)^6$] indicate that the on-site chemical shifts are decoupled to quadratic order. Analogous calculations with first-order pulses[27, 39] $S_1(\pi)$ and $S_1(\pi/2)$ give 1st-order [infidelity $\propto (\tau_p \Delta)^4$] decoupling and two orders of magnitude higher infidelities (not shown); Gaussian pulses increase infidelities by up to five orders of magnitude depending on the width.

bilizer generators, $G_x = \sigma_1^x \sigma_2^x \sigma_3^x \sigma_4^x$ and $G_z = \sigma_1^z \sigma_2^z \sigma_3^z \sigma_4^z$. We use the following explicit map (up to normalization)

$$\begin{aligned} |\tilde{0}\tilde{0}\rangle &= |0000\rangle + |1111\rangle, & |\tilde{0}\tilde{1}\rangle &= |0011\rangle + |1100\rangle, \\ |\tilde{1}\tilde{0}\rangle &= |0101\rangle + |1010\rangle, & |\tilde{1}\tilde{1}\rangle &= |0110\rangle + |1001\rangle, \end{aligned} \quad (6)$$

where digits with tildes indicate the states of the logical qubits. An application of any single-qubit error, i.e., a Pauli operator σ_i^μ , $\mu = x, y, z$, takes the encoded wavefunction to one of the three orthogonal subspaces, where one or both of the eigenvalues of G_x, G_z (these eigenvalues form the *error syndrome*) equal -1 . The code has distance $d = 2$ since some two-qubit errors, e.g., $\sigma_1^z \sigma_2^z$, act within the code space and cannot be detected.

In the presence of the error Hamiltonian (3), to leading order in the perturbation, the original wavefunction ψ_0 evolves into a superposition of orthogonal terms $A_0 |\psi_0\rangle + A_i^\mu \sigma_i^\mu |\psi_0\rangle$, where, in general, the coefficients are operators acting on the bath degrees of freedom, and the state fidelity is $F \equiv \text{Tr}_B (A_0^\dagger A_0 \rho_B)$, where trace over bath degrees of freedom with the density matrix ρ_B is taken. With the same accuracy, F is also the probability that the measurement returns $G_x = G_z = 1$. For weak perturbation, and for times t small compared to the bath correlation time τ_c , the infidelity $1 - F$ scales quadratically with t ; thus frequent projective measurements of the generators ensure preservation of the wavefunction with high probability (quantum Zeno effect[36, 37]).

Using the constructed DD-based gates, we simulated the encoding/decoding and ancilla-based stabilizer measurement circuits (Figs. 4, 5), where we use standard quantum circuit notations[49, 50]. The Hadamard gate was implemented using the identity $U_H = e^{-i\pi/2} \exp(i\frac{\pi}{4}\sigma_y) \exp(i\frac{\pi}{2}\sigma_x)$, and a projective

single-qubit measurement was implemented simply as an instantaneous projection to the state $|0\rangle$ of the ancilla.

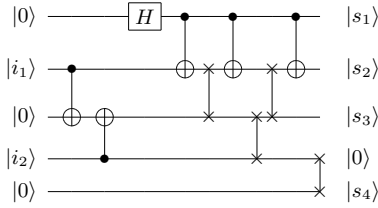


FIG. 4. Encoding circuit implemented on a spin chain using four exchange gates (implemented with three CNOTs each), five CNOT gates, and a Hadamard gate H . Input qubits i_1 , i_2 can be in an arbitrary two-qubit state, on the output the circuit returns an equivalent linear combination of the states in the code, see Eq. (6), using qubits s_j , $j = 1, \dots, 4$, and an ancilla initialized for the stabilizer measurement circuit in Fig. 5. The decoding is done by reversing this circuit.

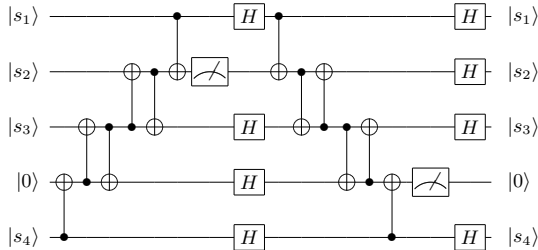


FIG. 5. Measurement circuit implemented on a spin chain with a shuttling ancilla. The ancilla is first shuttled up for the G_z measurement and then shuttled down for the G_x measurement (see text). The entire circuit is repeated for every Zeno cycle.

Samples of the simulation results are shown in Figs. 6, 7 which show the time-dependence of average infidelities and accumulated circuit failure probability, averaged over 20 instances of the classical correlated noise. The time axis starts at the end of the encoding circuit, see Fig. 4. Closed symbols represent the computed infidelity after the syndrome measurement (two points per circuit in Fig. 5); open symbols at the end of the final decoding (reverse of the circuit in Fig. 4). Blue squares stand for complete simulation, red circles have the pulses but no projection (dynamical decoupling is done but no Zeno effect happens, increasing the infidelity in our simulations by up to an order of magnitude), and black triangles where neither the decoupling pulses nor ancilla measurements are applied.

It is clear that the dynamical decoupling and the Zeno effect are both contributing to improving the fidelity, and both get better with decreasing noise. This indicates that the errors contributing to the infidelity of the constructed gates are not dominated by high-weight errors which would be undetectable by the code[51].

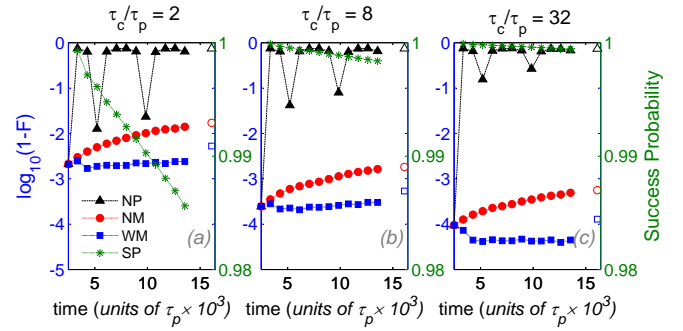


FIG. 6. (color online) Infidelities during the Zeno cycle for different noise correlation times as shown, with the same noise amplitude $\sigma = 10^{-3}/\tau_p$. The different curves correspond to cases where no pulses are applied (NP), DD pulses are applied but no measurements are done (NM), and with the syndrome measurements (WM). Note that the axis for the cumulative success probability (SP) of no error is on the right.

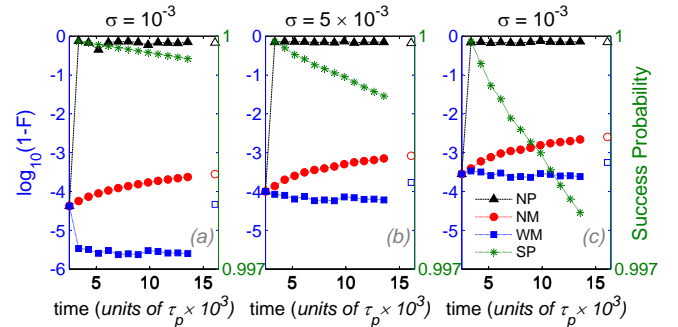


FIG. 7. (color online) Same as Fig. 6 but with fixed noise correlation time $\tau_c = 128\tau_p$ with the r.m.s. noise amplitudes σ as indicated.

The infidelity sharply increases with shorter noise correlation times; this results from the asymmetry of the DCGs, see Fig. 2. We have also constructed[51] symmetrized DCGs which give second-order decoupling for arbitrary bath operators B_i when used with the pulses constructed in Ref. 40; we expect such gates to have a much better accuracy for smaller noise correlation time, down to the gate duration, $\tau_c \geq 32\tau_p$.

IN CONCLUSION, we implemented a universal set of one- and two-qubit gates for a system with always-on qubit coupling. The gates are based on DD techniques and have an added benefit of protection against low-frequency phase noise.

One application of thus constructed gates is for implementing toric codes on square lattice, where one sublattice would be used for actual qubits, and the other sublattice for ancillas. This way, measurement of the entire syndrome can be done in just two cycles, each of four CNOTs in duration, plus some single-qubit gates. The same sequences would also work for an arbitrary quantum LDPC code, if the couplings between the qubits and the ancillas form the corresponding Tanner graph[52]. In particular, for hypergraph-product and related codes[34, 35]

one can use the square lattice layout with additional connections[53].

We are grateful to Kaveh Khodjasteh, Daniel Lidar, and Lorenza Viola for explaining the working of DCGs. This work was supported in part by the U.S. Army Research Office under Grant No. W911NF-11-1-0027, and by the NSF under Grant No. 1018935.

-
- [1] P. W. Shor, Phys. Rev. A, **52**, R2493 (1995).
- [2] E. Knill and R. Laflamme, Phys. Rev. A, **55**, 900 (1997).
- [3] C. Bennett, D. DiVincenzo, J. Smolin, and W. Wootters, Phys. Rev. A, **54**, 3824 (1996).
- [4] E. Knill, R. Laflamme, and W. H. Zurek, Science, **279**, 342 (1998).
- [5] E. Dennis, A. Kitaev, A. Landahl, and J. Preskill, J. Math. Phys., **43**, 4452 (2002).
- [6] A. M. Steane, Phys. Rev. A, **68**, 042322 (2003)
- [7] A. G. Fowler, C. D. Hill, and L. C. L. Hollenberg, Phys. Rev. A, **69**, 042314 (2004).
- [8] A. G. Fowler, S. J. Devitt, and L. C. L. Hollenberg, Quant. Info. Comput., **4**, 237 (2004), quant-ph/0402196.
- [9] R. Raussendorf and J. Harrington, Phys. Rev. Lett., **98**, 190504 (2007).
- [10] A. Y. Kitaev, Ann. Phys., **303**, 2 (2003).
- [11] L. M. K. Vandersypen and I. L. Chuang, Reviews of Modern Physics, **76**, 1037 (2004).
- [12] B. Criger, G. Passante, D. Park, and R. Laflamme, 10.1098/rsta.2011.0352 Philosophical Transactions of the Royal Society A: Mathematical, Physical and Engineering Sciences, **370**, 4620 (2012).
- [13] L. Viola, S. Lloyd, and E. Knill, Phys. Rev. Lett., **83**, 4888 (1999).
- [14] J. A. Jones and E. Knill, J. Mag. Res., **141**, 322 (1999).
- [15] L. Viola, Phys. Rev. A, **66**, 012307 (2002).
- [16] L. Viola and E. Knill, Phys. Rev. Lett., **90**, 037901 (2003).
- [17] K. Khodjasteh and D. A. Lidar, Phys. Rev. Lett., **95**, 180501 (2005).
- [18] G. S. Uhrig, Phys. Rev. Lett., **98**, 100504 (2007).
- [19] A. M. Souza, G. A. Álvarez, and D. Suter, 10.1103/PhysRevLett.106.240501 Phys. Rev. Lett., **106**, 240501 (2011).
- [20] J. A. Jones, Prg. Nucl. Mag. Res. Sp., **38**, 328 (2001).
- [21] E. M. Fortunato, M. A. Pravia, N. Boulant, G. Teklemariam, T. F. Havel, and D. G. Cory, 10.1063/1.1465412 The Journal of Chemical Physics, **116**, 7599 (2002).
- [22] M. D. Price, S. S. Somaroo, A. E. Dunlop, T. F. Havel, and D. G. Cory, Phys. Rev. A, **60**, 2777 (1999).
- [23] M. D. Price, S. S. Somaroo, C. H. Tseng, J. C. Gore, A. H. Fahmy, T. F. Havel, and D. G. Cory, J. Mag. Res., **140**, 371 (1999).
- [24] M. D. Price, T. F. Havel, and D. G. Cory, New J. Phys., **2**, 10 (2000).
- [25] J. J. Vartiainen, A. O. Niskanen, M. Nakahara, and M. M. Salomaa, Phys. Rev. A, **70**, 012319 (2004).
- [26] C. P. Slichter, *Principles of Magnetic Resonance*, 3rd ed. (Springer-Verlag, New York, 1992).
- [27] P. Sengupta and L. P. Pryadko, Phys. Rev. Lett., **95**, 037202 (2005)
- [28] L. P. Pryadko and P. Sengupta, Phys. Rev. B, **73**, 085321 (2006).
- [29] M. Stollsteimer and G. Mahler, Phys. Rev. A, **64**, 052301 (2001).
- [30] Y. Tomita, J. T. Merrill, and K. R. Brown, New J. Phys., **12**, 015002 (2010).
- [31] K. Khodjasteh and L. Viola, Phys. Rev. Lett., **102**, 080501 (2009).
- [32] M. S. Postol, (2001), unpublished, <http://arxiv.org/abs/arXiv:quant-ph/0108131v1> arXiv:quant-ph/0108131v1.
- [33] D. J. C. MacKay, G. Mitchison, and P. L. McFadden, IEEE Transactions on Information Theory, **59**, 2315 (2004).
- [34] J.-P. Tillich and G. Zemor, in 10.1109/ISIT.2009.5205648 *Information Theory, 2009. ISIT 2009. IEEE International Symposium on* (2009) pp. 799–803.
- [35] A. A. Kovalev and L. P. Pryadko, in 10.1109/ISIT.2012.6284206 *Information Theory Proceedings (ISIT), 2012 IEEE International Symposium on* (2012) pp. 348–352, ISSN 2157-8095, <http://arxiv.org/abs/arXiv:1202.0928> arXiv:1202.0928.
- [36] P. Facchi and S. Pascazio, Phys. Rev. Lett., **89**, 080401 (2002).
- [37] P. Facchi, S. Pascazio, A. Scardicchio, and L. S. Schulman, Phys. Rev. A, **65**, 012108 (2002).
- [38] W. S. Warren, J. Chem. Phys., **81**, 5437 (1984).
- [39] L. P. Pryadko and P. Sengupta, 10.1103/PhysRevA.78.032336 Phys. Rev. A, **78**, 032336 (2008).
- [40] S. Pasini, T. Fischer, P. Karbach, and G. S. Uhrig, Phys. Rev. A, **77**, 032315 (2008).
- [41] L. P. Pryadko and G. Quiroz, Phys. Rev. A, **77**, 012330/1 (2007).
- [42] K. Khodjasteh and L. Viola, Phys. Rev. A, **80**, 032314 (2009).
- [43] K. Khodjasteh, D. A. Lidar, and L. Viola, 10.1103/PhysRevLett.104.090501 Phys. Rev. Lett., **104**, 090501 (2010).
- [44] G. Lindblad, Commun. Math. Phys., **48**, 119 (1976).
- [45] A. Galiutdinov and M. Geller, (2007), arXiv:quant-ph/0703208v1.
- [46] G. Guennebaud, B. Jacob, *et al.*, Eigen v3, <http://eigen.tuxfamily.org> (2010).
- [47] M. Grassl, T. Beth, and T. Pellizzari, 10.1103/PhysRevA.56.33 Phys. Rev. A, **56**, 33 (1997).
- [48] D. Gottesman, *Stabilizer Codes and Quantum Error Correction*, Ph.D. thesis, Caltech (1997).
- [49] M. A. Nielsen and I. L. Chuang, *Quantum Computation and Quantum Information* (Cambridge Unive. Press, Cambridge, MA, 2000).
- [50] A. Barenco, C. H. Bennett, R. Cleve, D. P. DiVincenzo, N. Margolus, P. Shor, T. Sleator, J. A. Smolin, and H. Weinfurter, Phys. Rev. A, **52**, 3457 (1995).
- [51] A. De and L. P. Pryadko, (2012), unpublished.
- [52] R. Tanner, Information Theory, IEEE Transactions on, **27**, 533 (1981).
- [53] A. A. Kovalev and L. P. Pryadko, (2012), <http://arxiv.org/abs/arXiv:1208.2317> arXiv:1208.2317